

Generation of amorphous carbon and crystallographic texture during low-temperature subseismic slip in calcite fault gouge

Claudio Delle Piane^{1*}, Sandra Piazzolo^{2,3}, Nicholas E. Timms⁴, Vladimir Luzin⁵, Martin Saunders⁶, Julien Bourdet¹, Ausama Giwelli¹, M. Ben Clennell¹, Charlie Kong⁷, William D.A. Rickard⁸, and Michael Verrall⁹

¹CSIRO Energy, Kensington, WA 6151, Australia

²Australian Research Council Centre of Excellence for Core to Crust Fluid Systems/GEMOC, Department of Earth and Planetary Sciences, Macquarie University, Sydney, NSW 2109, Australia

³School of Earth and Environment, University of Leeds, Leeds LS2 9JT, UK

⁴Department of Applied Geology, Curtin University, Perth, WA 6102, Australia

⁵Australian Nuclear Science and Technology Organization, Lucas Heights, NSW 2234, Australia

⁶Centre for Microscopy, Characterization & Analysis, University of Western Australia, M010, Perth, WA 6009, Australia

⁷Electron Microscope Unit, University of New South Wales, Sydney, NSW 2052, Australia

⁸Advanced Resource Characterization Facility, John de Laeter Centre, Curtin University, Perth, WA 6102, Australia

⁹CSIRO, Mineral Resources, Perth, WA 6151, Australia

ABSTRACT

Identification of the nano-scale to micro-scale mechanochemical processes occurring during fault slip is of fundamental importance to understand earthquake nucleation and propagation. Here we explore the micromechanical processes occurring during fault nucleation and slip at subseismic rates ($\sim 3 \times 10^{-6} \text{ m s}^{-1}$) in carbonate rocks. We experimentally sheared calcite-rich travertine blocks at simulated upper crustal conditions, producing a nano-grained fault gouge. Strain in the gouge is accommodated by cataclastic comminution of calcite grains and concurrent crystal-plastic deformation through twinning and dislocation glide, producing a crystallographic preferred orientation (CPO). Continued wear of fine-grained gouge particles results in the mechanical decomposition of calcite and production of amorphous carbon. We show that CPO and the production of amorphous carbon, previously attributed to frictional heating and weakening during seismic slip, can be produced at low temperature during stable slip at subseismic rates without slip weakening.

INTRODUCTION

Carbonate rocks in the upper crust host hypocenters of medium to large earthquakes worldwide and studies conducted on exhumed carbonate-hosted faults indicate that coseismic slip is accommodated within highly localized slip zones a few millimeters thick, filled with fault gouge. These slip zones are characterized by the presence of nano-scale grains (Simantov et al., 2013), the occurrence of decarbonation products and amorphous phases linked to frictional heating (Collettini et al., 2014), and crystallographic preferred orientation (CPO) (Smith et al., 2013). Elucidating the conditions and nano-scale to micro-scale deformation mechanisms that control the occurrence of these microstructural features and how they relate to the frictional behavior of the fault gouge during seismic and subseismic slip is crucial for understanding the processes leading to earthquake slip in carbonate rocks.

Here we present a microstructural and nanostructural analysis of experimentally deformed calcite gouge to identify the fundamental processes occurring during subseismic slip at conditions mimicking the interseismic period in upper crustal carbonate faults. We monitor the frictional response of the rock as a function of shear displacement during direct shear experiments and use a range of microanalytical techniques including

neutron diffraction, high-resolution scanning electron microscopy (SEM) imaging, electron backscatter diffraction (EBSD), transmission Kikuchi diffraction (TKD), transmission electron microscopy (TEM), electron energy loss spectroscopy (EELS), and microfocused Raman spectroscopy for quantitative microstructural characterization. Our results show that deformation at subseismic slip rates is accommodated by a combination of cataclastic grain comminution, crystal-plastic deformation by twinning and dislocation glide, and mechanically activated dissociation of calcite leading to generation of amorphous carbon, simultaneously occurring without changes in bulk frictional properties of the fault zone.

METHODS

Direct shear experiments were conducted on water-saturated intact blocks of travertine (with dimensions of $24 \times 11 \times 15 \text{ cm}^3$) sourced from a quarry in the central Apennines in Italy. The starting material was composed of 99 wt% calcite, as determined by quantitative X-ray diffraction analysis. Trace amounts ($0.16 \pm 0.11 \text{ wt\%}$) of organic carbon were identified using conventional pyrolytic tests.

Direct shear tests were conducted at subseismic slip rates of $3\text{--}17 \times 10^{-6} \text{ m s}^{-1}$ under a maximum normal stress of 45 MPa, and ambient laboratory temperature of $\sim 25 \text{ }^\circ\text{C}$ (Giwelli et al., 2016). Shear (τ) and normal (σ) stresses are recorded allowing derivation of the friction coefficient ($\mu = \sigma/\tau$). To study the evolution of the microstructure in the gouge as a function of progressive deformation, several samples were sheared to different maximum displacements of 20, 70, and 120 mm, and subsequently studied via optical, neutron and electron based analytical techniques (see the GSA Data Repository¹ for methodology).

MICROSTRUCTURAL EVOLUTION WITH SLIP

Direct shear experiments consistently showed rapid, near-linear loading followed by hardening toward a peak μ of ~ 0.8 . With increasing slip μ decreased to values of 0.55–0.6 and remained nearly constant up to displacements of $\sim 70 \text{ mm}$ (Fig. 1A). At higher displacements, the measured friction is affected by the increasing contact area between the sample and

¹GSA Data Repository item 2018037, Items DR1 (image analysis of sheared samples), DR2 (travertine textural characterization), DR3 (TKD and TEM procedure), DR4 (calculation of friction heat rise during shearing), and DR5 (EDS and Raman analysis of gouge and identification of amorphous carbon), is available online at <http://www.geosociety.org/datarepository/2018/> or on request from editing@geosociety.org.

*E-mail: Claudio.Dellepiane@csiro.au

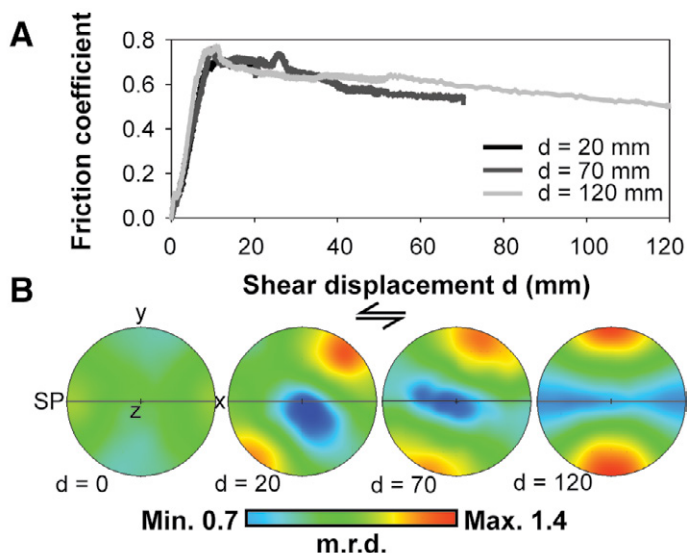


Figure 1. A: Evolution of friction coefficient as a function of shear displacement (d) in the travertine samples used in this study. **B:** Calcite (006) pole figures measured via neutron diffraction on cohesive wafers of gouge extracted from blocks sheared to different amount of shear displacement (d , in mm). SP—shear plane. Color bar is in multiple of random distribution (m.r.d.). Max.—maximum; Min.—minimum.

the low-friction Teflon gasket used to seal the direct shear box (Giwelli et al., 2016). Macroscopic observations on the sheared blocks indicate that deformation is first accommodated in a shear zone (~15 mm wide) forming after 20 mm of slip; as slip progresses, deformation localizes into gouge layers (~10 mm wide) of extremely reduced grain sizes (Delle Piane et al., 2016). Quantitative image analysis of gouge particles based on SEM images revealed that the resolvable grain sizes typically range between 10 nm and ~5 μm . Increasing shear displacement from 20 to 120 mm results in the grains become smaller and more rounded (see Item DR1 in the Data Repository).

Textural analysis by neutron diffraction and EBSD analysis indicates a preexisting weak CPO in the intact travertine characterized by alignment of calcite c -axes normal to the sedimentary bedding (Item DR2). This CPO was destroyed upon initial shearing, and a different deformation-induced CPO evolved rapidly in the gouge with progressive slip. Distinct maxima in poles to the (006) diffraction band (parallel to the c -axis in calcite) developed at high angles (60° – 90°) to the shear plane after low finite displacement (20 mm slip), and rotated progressively to be orthogonal to the shear direction by 120 mm slip (Fig. 1B).

During initial shearing, large relict calcite clasts close to fractures develop e -twins; within the gouge zone, TKD analysis revealed that calcite clasts that are $<5 \mu\text{m}$ across mainly comprise single grains of calcite with abundant e -twins (Fig. 2A) and lack the straight subgrain boundaries observed in the undeformed primary sparry crystals (Item DR2). Clasts as small as 200 nm preserve deformation-induced crystal-plastic microstructures where individual grains show significant continuous lattice distortion that typically accommodates as much as 5° of cumulative intracrystal orientation change over length scales of ~500 nm (Fig. 2B). The areas between grains that did not produce coherent diffraction patterns during TKD analysis are predominantly composed of carbon, as revealed by energy-dispersive X-ray spectroscopy elemental mapping, have distinctive EELS and Raman spectra (Item DR5), and are therefore identified as amorphous carbonaceous material (black areas in Fig. 2A).

TEM images from a foil extracted from the gouge zone show that calcite particles in the 0.5–2- μm -diameter range are generally equant to slightly elongate and characterized by a heterogeneous dislocation density, with almost defect-free cores and significantly higher dislocation densities along the rims (Fig. 3A). There is a large population of small (50 nm

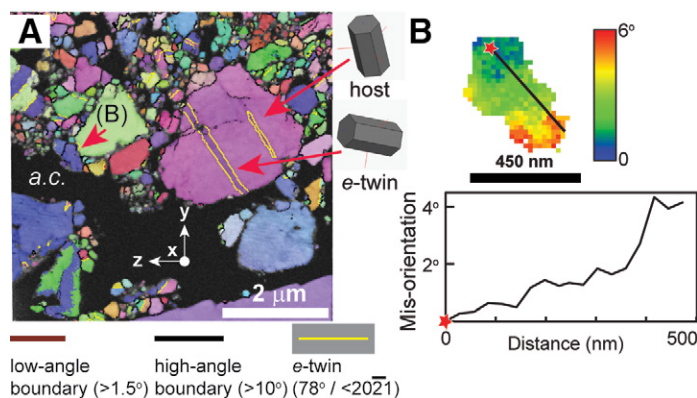


Figure 2. Characteristic deformation microstructure of the sheared travertine. A: Transmission Kikuchi diffraction (TKD) map in all Euler color scheme with overlain grain boundary map showing calcite grains of various size with internal distortion and deformation twins. Also shown are the schematic relationships between twin and host grains. Areas of amorphous carbon (a.c.) do not yield diffraction patterns and appear black. **B:** Misorientation map and profile of a calcite grain showing deformation-induced internal crystallographic distortion of 5° over a length of 450 nm.

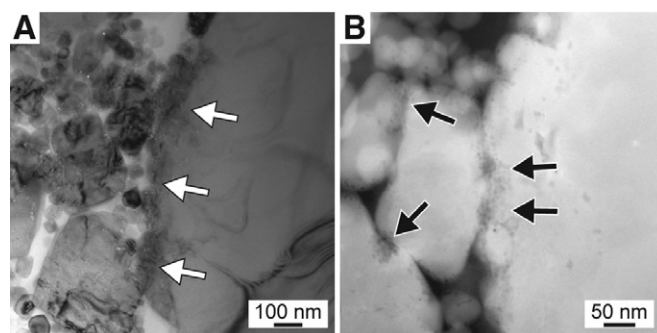


Figure 3. Transmission electron microscope (TEM) images of gouge particles produced after 120 mm of shear displacement. A: Micrometer-sized calcite crystal surrounded by a submicrometer matrix. Note the difference in dislocation density between the core and the rim of the crystals (white arrows). **B:** High-angle annular dark-field scanning TEM image of grain-grain contacts (black arrows) decorated by degassing vesicles (small black dots, each ~5 nm across).

diameter) calcite particles that are also equant, and have rhombohedral or hexagonal forms (Figs. 3A and 3B). Boundaries of these clasts are irregular and decorated with voids (~5 nm across), which are particularly abundant at clast-clast contacts (Fig. 3B).

EELS spectra characterize the bonding structure of the particles in the gouge and reveal the coexistence of calcite and amorphous carbon (Fig. 4). Calcite grains show a characteristic sharp peak at 290 eV and a broader, less intense feature with maximum at 300 eV, well-developed Ca $L_{2,3}$ edge at ~350 eV, and O-K-edge at ~540 eV (Benzerara et al., 2005; Garvie et al., 1994) (Fig. 4B). Further peaks at 286 eV and at 532 eV cannot be assigned to carbonate bonds, and are indicative of carbonyl or carboxyl groups (Benzerara et al., 2005). In the carbon-rich areas, EELS spectra show C-K edge structures characterized by a 285 eV (π^*) peak, a second more intense, broad feature at ~295 eV (σ^* peak), and a broader multiple scattering resonance peak at ~330 eV diagnostic of amorphous carbon (Daniels et al., 2007). Minor peaks are related to the presence of Ca (~350 eV) and O (~540 eV), consistent with minor relict calcite (Fig. 4C).

DISCUSSION

Throughout experiments, early deformation is dominated by grain fracturing followed by abrasion-dominated comminution. During early

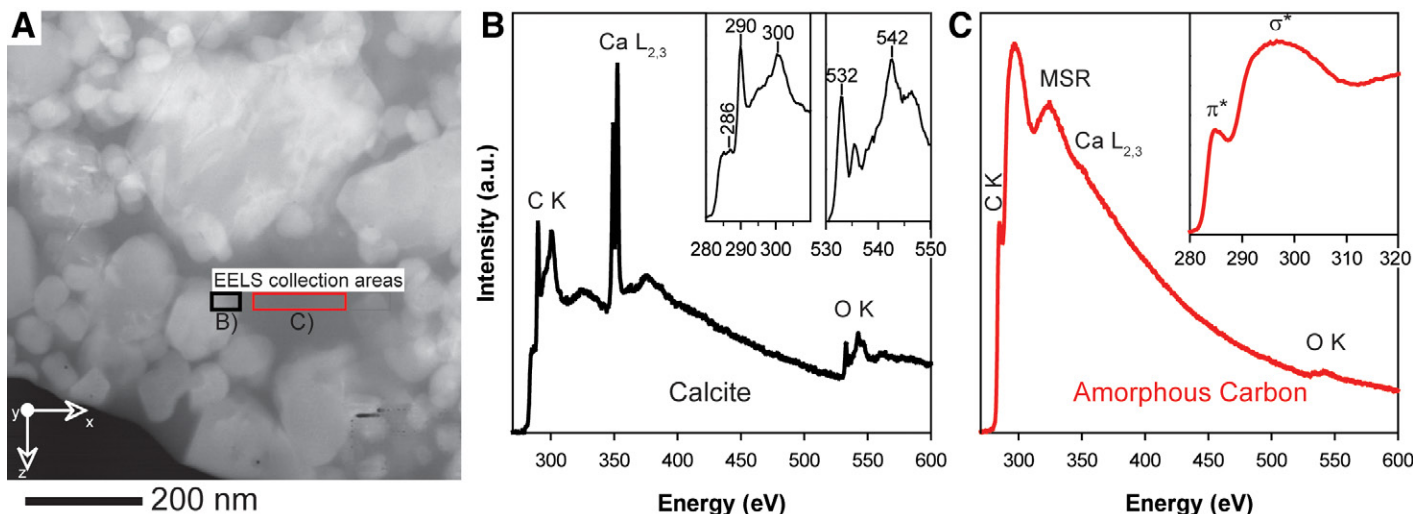


Figure 4. A: High-angle annular dark-field scanning transmission electron microscopy image of a gouge region used for collection of electron energy loss spectroscopy (EELS) spectra. B: EELS spectrum averaged over the black box shown in A with peaks and edges associated with calcite and carbonyl or carboxyl groups (see text for details). C: EELS spectrum averaged over the red box shown in A with features typical of amorphous carbon (π^* peak and σ^* peak). MSR—multiple scattering resonance.

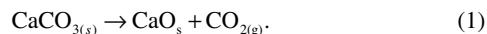
fracture-dominated cataclasis, random rotation of comminuted clasts quickly destroyed the primary calcite CPO of the travertine. The development of a new CPO, along with the localized high dislocation density, lattice distortion, and twin generation indicate that crystal plasticity played a significant role in accommodating deformation during the experiments. The deformation-induced CPO is attributed to intracrystalline slip on the *r*-glide system in calcite and simultaneous *e*-twinning. The abundant *e*-twins in the gouge are deformation induced, because these are absent in the pre-deformation material. The simultaneous operation of *e*-twinning and dislocation glide on the *r*-glide system is consistent with low-temperature plasticity of calcite reported in laboratory experiments and exhumed carbonate faults (De Bresser and Spiers, 1997; Kennedy and White, 2001).

The presence of nanoscale calcite clasts in the gouge raises questions about their formation mechanism because theories of fracture propagation are limited to calcium carbonate particles larger than $\sim 1 \mu\text{m}$ (Kendall, 1978). However, calcite nanograins have been observed in natural fault rocks (Kennedy and White, 2001; Collettini et al., 2014) and in shear experiments on simulated gouges (Han et al., 2010; Tisato et al., 2012; Verberne et al., 2013, 2014; Toy et al., 2015; Delle Piane et al., 2016).

The high lattice distortion of the gouge grains is consistent with high stress deformation during shearing: point contacts between impinging grains acted as stress risers, locally activating dislocation glide. Dislocation glide in the gouge matrix during shearing resulted in dislocation networks organizing into a cell structure similar to that originating from low-temperature attrition milling (Rawers and Cook, 1999), whereupon the structural degradation of large grains follows the generation and multiplication of dislocations associated with stress risers at grain boundaries during particle impingement. The newly generated dislocations interacted to form cell walls at grain boundaries evolving into nanoscopic grains (Fig. 3A) similar to those described by De Paola et al. (2015).

Analyses by TKD, EELS, and Raman spectroscopy corroborate that high concentrations (to 50% by area) of amorphous carbon were produced in the gouge at low-temperature and subseismic slip conditions (Figs. 2 and 4). The close spatial proximity of calcite point contacts, nanovesicles, and interstitial amorphous carbon (Fig. 3B) suggests a causal link between these microstructural components. It is interesting that the nanoscale vesicles closely resemble those associated with thermal decarbonation of calcite (Collettini et al., 2013). For the experimental conditions used, the temperature rise (ΔT) due to frictional heating, calculated following

Rice (2006) and using typical parameters for calcite (Item DR4), ranges between 4 and 13 °C. Therefore, the temperature within the gouge was calculated to remain <50 °C, well below the values required for the initiation of thermal decarbonation (~ 600 °C, according to Rodriguez-Navarro et al., 2009). Thus, the mechanism of decarbonation requires an alternative explanation to frictional heating. The presence of decarbonation vesicles could be explained by the mechanochemical dissociation of calcite (Dickinson et al., 1991; Martinelli and Plescia, 2004) resulting from high stress concentration at clast-clast point contacts. Stored strain energy associated with high dislocation density near the surfaces of the comminuted clasts can facilitate the dissociation by reducing the effective energy barrier for reaction (Yue et al., 1999). In this scenario, the dissociation would liberate gaseous CO_2 responsible for the observed vesicles according to the reaction:



Previous experimental studies on simulated calcite gouges sheared at seismic velocity ($\sim 1 \text{m s}^{-1}$) reported the occurrence of amorphous carbon and graphite attributed to thermal decomposition of calcite and ensuing precipitation of carbon via high-temperature gas reactions and thermochemical vapor deposition (Oohashi et al., 2014; Spagnuolo et al., 2015).

The formation of amorphous carbon at low temperature during faulting in carbonates is an unexpected result of our study and requires an alternative mechanism to produce free carbon without thermal decomposition. Geochemical evidence points to the precipitation of carbonaceous solids from a C-O-H-rich pore fluid (Luque et al., 1998). We propose that CO_2 liberated by the mechanically activated dissociation and decarbonation of calcite saturates the pore water with respect to carbon, which is then precipitated in an amorphous state and as carbonyl or carboxyl groups, as indicated by the EELS results (Fig. 4).

Amorphous carbon has been previously linked to dramatic dynamic weakening in high-velocity friction experiments on calcite gouges (Spagnuolo et al., 2015). However, we note that our slow slip tests indicate that the friction coefficient of the gouge was not affected by the development of amorphous carbon, at least in the volumetric proportions that we observed. This is in agreement with the results of Oohashi et al. (2011) reporting large differences in steady-state friction coefficient of amorphous carbon at low ($\mu = 0.54$) and high ($\mu = 0.1$) slip rates.

Therefore, at subseismic slip rates, deformation in calcite-dominated rocks is accommodated by grain-size reduction through brittle cataclasis, grain comminution, and crystal-plastic deformation, development of

CPO through *e*-twin generation and *r*-slip, and mechanical, rather than thermally activated, dissociation of calcite resulting in the generation of amorphous carbon. It is important that the development of these microstructural features occurs during stable sliding with negligible frictional heating and without dramatic weakening.

Amorphous carbon generated during low-temperature subseismic faulting of carbonates is a previously unrecognized source of carbonaceous material in fault zones available for subsequent transformation into graphite, which is known to occupy the principal slip surfaces of many faults and shear zones, and acts as a solid natural lubricant for slip due to its extremely low coefficient of friction of ~0.1 (Oohashi et al., 2012).

ACKNOWLEDGMENTS

We acknowledge the support of the Australian Centre for Neutron Scattering, Australian Nuclear Science and Technology Organization, in providing the neutron research facilities used in this work. We acknowledge the facilities and the scientific and technical assistance of the Australian Microscopy and Microanalysis Research Facility at the Centre for Microscopy, Characterization and Analysis, University of Western Australia, funded by the University, State, and Commonwealth Governments. The Tescan Lyra FIB-SEM (focused ion beam-scanning electron microscope) used in this study is part of the Advanced Resource Characterization Facility (ARCF). The ARCF, under the auspices of the National Resource Sciences Precinct (NRSP), a collaboration between the Commonwealth Scientific and Industrial Research Organisation (CSIRO), Curtin University, and The University of Western Australia, is supported by the Science and Industry Endowment Fund. Laboratory experiments on travertine were conducted with funding from Petrobras, Brazil, as part of the project Fault Reactivation in Carbonate Reservoirs. We acknowledge the contributions of the project team in producing the fault gouge materials examined in this work. We thank Mark Pearce for stimulating important discussion on carbon generation and David N. Dewhurst for his critical reading of an earlier version of the manuscript. We thank the editor Mark Quigley and three anonymous reviewers for their helpful feedback.

REFERENCES CITED

Benzerara, K., Menguy, N., Guyot, F., Vanni, C., and Gillet, P., 2005, TEM study of a silicate-carbonate-microbe interface prepared by focused ion beam milling: *Geochimica et Cosmochimica Acta*, v. 69, p. 1413–1422, <https://doi.org/10.1016/j.gca.2004.09.008>.

Collettini, C., Viti, C., Tesei, T., and Mollo, S., 2013, Thermal decomposition along natural carbonate faults during earthquakes: *Geology*, v. 41, p. 927–930, <https://doi.org/10.1130/G34421.1>.

Collettini, C., Carpenter, B.M., Viti, C., Cruciani, F., Mollo, S., Tesei, T., Trippetta, F., Valoroso, L., and Chiaraluce, L., 2014, Fault structure and slip localization in carbonate-bearing normal faults: An example from the Northern Apennines of Italy: *Journal of Structural Geology*, v. 67, p. 154–166, <https://doi.org/10.1016/j.jsg.2014.07.017>.

Daniels, H., Brydson, R., Rand, B., and Brown, A., 2007, Investigating carbonization and graphitization using electron energy loss spectroscopy (EELS) in the transmission electron microscope (TEM): *Philosophical Magazine*, v. 87, p. 4073–4092, <https://doi.org/10.1080/14786430701394041>.

De Bresser, J.H.P., and Spiers, C.J., 1997, Strength characteristics of the *r*, *f*, and *c* slip systems in calcite: *Tectonophysics*, v. 272, p. 1–23, [https://doi.org/10.1016/S0040-1951\(96\)00273-9](https://doi.org/10.1016/S0040-1951(96)00273-9).

Delle Piane, C., Giwelli, A., Clennell, M.B., Esteban, L., Kiewiet, M.C.D.N., Kiewiet, L., Kager, S., and Raimon, J., 2016, Frictional and hydraulic behaviour of carbonate fault gouge during fault reactivation—An experimental study: *Tectonophysics*, v. 690, p. 21–34, <https://doi.org/10.1016/j.tecto.2016.07.011>.

De Paola, N., Holdsworth, R.E., Viti, C., Collettini, C., and Bullock, R., 2015, Can grain size sensitive flow lubricate faults during the initial stages of earthquake propagation?: *Earth and Planetary Science Letters*, v. 431, p. 48–58, <https://doi.org/10.1016/j.epsl.2015.09.002>.

Dickinson, J.T., Jensen, L.C., Langford, S.C., Rosenberg, P.E., and Blanchard, D.L., 1991, CO₂ emission accompanying the fracture of calcite: *Physics and Chemistry of Minerals*, v. 18, p. 320–325, <https://doi.org/10.1007/BF00200189>.

Garvie, L.A.J., Craven, A.J., and Brydson, R., 1994, Use of electron-energy loss near-edge fine structure in the study of minerals: *American Mineralogist*, v. 79, p. 411–425.

Giwelli, A., Delle Piane, C., Esteban, L., Clennell, M.B., Dautriat, J., Raimon, J., Kager, S., and Kiewiet, L., 2016, Laboratory observations of fault transmissibility

alteration in carbonate rock during direct shearing: *Geofluids*, v. 16, p. 658–672, <https://doi.org/10.1111/gfl.12183>.

Han, R., Hirose, T., and Shimamoto, T., 2010, Strong velocity weakening and powder lubrication of simulated carbonate faults at seismic slip rates: *Journal of Geophysical Research*, v. 115, B03412, <https://doi.org/10.1029/2008JB006136>.

Kendall, K., 1978, The impossibility of comminuting small particles by compression: *Nature*, v. 272, p. 710–711, <https://doi.org/10.1038/272710a0>.

Kennedy, L.A., and White, J.C., 2001, Low-temperature recrystallization in calcite: Mechanisms and consequences: *Geology*, v. 29, p. 1027–1030, [https://doi.org/10.1130/0091-7613\(2001\)029<1027:LTRICM>2.0.CO;2](https://doi.org/10.1130/0091-7613(2001)029<1027:LTRICM>2.0.CO;2).

Luque, F.J., Pasteris, J.D., Wopenka, B., Rodas, M., and Barrenechea, J.F., 1998, Natural fluid deposited graphite: Mineralogical characteristics and mechanisms of formation: *American Journal of Science*, v. 298, p. 471–498, <https://doi.org/10.2475/ajs.298.6.471>.

Martinelli, G., and Plešcia, P., 2004, Mechanochemical dissociation of calcium carbonate: Laboratory data and relation to natural emissions of CO₂: *Physics of the Earth and Planetary Interiors*, v. 142, p. 205–214, <https://doi.org/10.1016/j.pepi.2003.12.009>.

Oohashi, K., Hirose, T., and Shimamoto, T., 2011, Shear-induced graphitization of carbonaceous materials during seismic fault motion: Experiments and possible implications for fault mechanics: *Journal of Structural Geology*, v. 33, p. 1122–1134, <https://doi.org/10.1016/j.jsg.2011.01.007>.

Oohashi, K., Hirose, T., Kobayashi, K., and Shimamoto, T., 2012, The occurrence of graphite-bearing fault rocks in the Atotsugawa fault system, Japan: Origins and implications for fault creep: *Journal of Structural Geology*, v. 38, p. 39–50, <https://doi.org/10.1016/j.jsg.2011.10.011>.

Oohashi, K., Han, R., Hirose, T., Shimamoto, T., Omura, K., and Matsuda, T., 2014, Carbon-forming reactions under a reducing atmosphere during seismic fault slip: *Geology*, v. 42, p. 787–790, <https://doi.org/10.1130/G35703.1>.

Rawers, J., and Cook, D., 1999, Influence of attrition milling on nano-grain boundaries: *Nanotechnology Materials*, v. 11, p. 331–342, [https://doi.org/10.1016/S0965-9773\(99\)00049-5](https://doi.org/10.1016/S0965-9773(99)00049-5).

Rice, J.R., 2006, Heating and weakening of faults during earthquake slip: *Journal of Geophysical Research*, v. 111, B05311, <https://doi.org/10.1029/2005JB004006>.

Rodríguez-Navarro, C., Ruiz-Agudo, E., Luque, A., Rodríguez-Navarro, A.B., and Ortega-Huertás, M., 2009, Thermal decomposition of calcite: Mechanisms of formation and textural evolution of CaO nanocrystals: *American Mineralogist*, v. 94, p. 578–593, <https://doi.org/10.2138/am.2009.3021>.

Siman-Tov, S., Aharonov, E., Sagy, A., and Emmanuel, S., 2013, Nanograins form carbonate fault mirrors: *Geology*, v. 41, p. 703–706, <https://doi.org/10.1130/G34087.1>.

Smith, S.A.F., Di Toro, G., Kim, S., Ree, J.H., Nielsen, S., Billi, A., and Spiess, R., 2013, Coseismic recrystallization during shallow earthquake slip: *Geology*, v. 41, p. 63–66, <https://doi.org/10.1130/G33588.1>.

Spagnuolo, E., Plümpner, O., Violay, M., Cavallo, A., and Di Toro, G., 2015, Fast-moving dislocations trigger flash weakening in carbonate-bearing faults during earthquakes: *Scientific Reports*, v. 5, 16112, <https://doi.org/10.1038/srep16112>.

Tisato, N., Di Toro, G., De Rossi, N., Quaresimin, M., and Candela, T., 2012, Experimental investigation of flash weakening in limestone: *Journal of Structural Geology*, v. 38, p. 183–199, <https://doi.org/10.1016/j.jsg.2011.11.017>.

Toy, V.G., Mitchell, T.M., Druiventak, A., and Wirth, R., 2015, Crystallographic preferred orientations may develop in nanocrystalline materials on fault planes due to surface energy interactions: *Geochemistry, Geophysics, Geosystems*, v. 16, p. 2549–2563, <https://doi.org/10.1002/2015GC005857>.

Verberne, B.A., de Bresser, J.H., Niemeijer, A.R., Spiers, C.J., de Winter, D.M., and Plümpner, O., 2013, Nanocrystalline slip zones in calcite fault gouge show intense crystallographic preferred orientation: Crystal plasticity at sub-seismic slip rates at 18–150 °C: *Geology*, v. 41, p. 863–866, <https://doi.org/10.1130/G34279.1>.

Verberne, B.A., Plümpner, O., de Winter, D.M., and Spiers, C.J., 2014, Superplastic nanofibrous slip zones control seismic friction: *Science*, v. 346, p. 1342–1344, <https://doi.org/10.1126/science.1259003>.

Yue, L., Shui, M., and Xu, Z., 1999, The decomposition kinetics of nanocrystalline calcite: *Thermochemica Acta*, v. 335, p. 121–126, [https://doi.org/10.1016/S0040-6031\(99\)00174-4](https://doi.org/10.1016/S0040-6031(99)00174-4).

Manuscript received 3 August 2017

Revised manuscript received 24 October 2017

Manuscript accepted 27 November 2017

Printed in USA